

Frequency shift in the oscillating cantilever-driven adiabatic reversals technique as a function of the spin location

G.P. Bernan,¹ F. Borgonovi,^{2,3} and V.I. Tsvetkovich⁴

¹Theoretical Division and CNLS, MS B213, Los Alamos National Laboratory, Los Alamos, NM 87545

²Dipartimento di Matematica e Fisica, Università Cattolica, via Musei 41, 25121 Brescia, Italy

³INFN, Unita di Brescia and INFN, Sezione di Pavia, Italy

⁴Department, Polytechnic University, Six Metrotech Center, Brooklyn, New York 11201

(Dated: January 26, 2020)

The theory of the oscillating cantilever-driven adiabatic reversals (OSCAR) in magnetic resonance force microscopy (MRFM) is extended for the arbitrary relation between the external and dipole magnetic fields and for arbitrary location of a single spin. The analytical estimate for the OSCAR MRFM frequency shift is derived and it is shown to be in excellent agreement with numerical simulations. The dependence of the frequency shift on the position of the spin relative to the cantilever has characteristic maxima and minima which can be used for the experimental detection of the spin location.

PACS numbers: 76.60.-k, 07.55.-w

I. INTRODUCTION

The oscillating cantilever driven adiabatic reversals (OSCAR) technique in magnetic resonance force microscopy (MRFM) introduced in [1] has been successfully implemented for the first detection of a single electron spin below the surface of a solid [2]. In the OSCAR MRFM technique the vibrations of the cantilever tip (CT) with an attached ferromagnetic particle in presence of a rf magnetic field cause the periodic reversals of the effective magnetic field acting on the single electron spin. If the conditions of adiabatic motion are satisfied the spin follows the effective magnetic field. The back action of the spin on the CT causes the small frequency shift of CT vibrations, which can be measured with high precision.

The quasiclassical theory of OSCAR MRFM has been developed in [3]. However, this theory contains two important limitations. First, it assumes that the external magnetic field B_{ext} on the spin is much greater than the dipole field B_d produced by the ferromagnetic particle. On the other hand, in real experiments, in order to increase the frequency shift Δ_f , one has to decrease the distance between the CT and the spin to values where the dipole field becomes sometimes greater than the external field [2]. Second, it was assumed in [3] that the spin is located in the plane of the cantilever vibrations. Thus, the quasiclassical theory should be extended in order to describe both an arbitrary relation between B_{ext} and B_d and an arbitrary location of the spin. This extension is presented in our paper.

One can argue that a single spin is a quantum object and must be described within the quantum theory frame. The quantum theory of OSCAR MRFM has been developed in [4] with the same limitations as the quasiclassical theory. It was found, as may be expected, that the frequency shift Δ_f in quantum theory may accept only two values $\pm \Delta_f$ corresponding to the two directions of spin

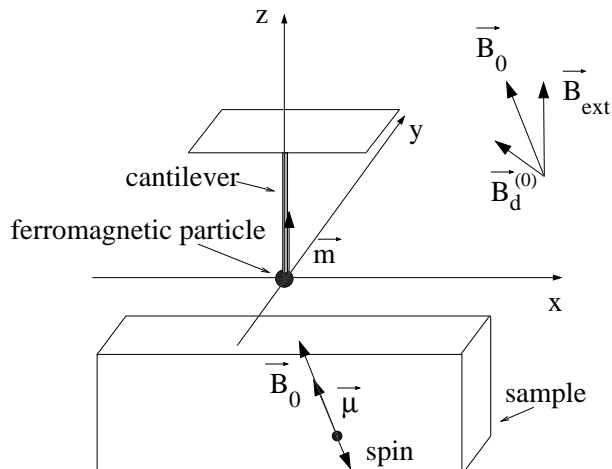


FIG. 1: MRFM setup. The equilibrium position of the spin and the cantilever with a spherical ferromagnetic particle. m is the magnetic moment of the ferromagnetic particle, μ is the magnetic moment of the spin, B_{ext} , $B_d^{(0)}$ and B_0 are respectively the external permanent magnetic field, the dipole field on the spin, and the net magnetic field. In general the vectors $B_d^{(0)}$ and B_0 do not lie in the $x-z$ plane.

relative to the effective magnetic field. The value $\pm \Delta_f$ in quantum theory is the same as the maximum frequency shift received in the quasiclassical theory (where it can take any value between $-\Delta_f$ and Δ_f). Thus, for frequency shift computation it is reasonable to use quasiclassical instead of quantum theory.

II. EQUATIONS OF MOTION

We consider the MRFM setup shown in Fig. 1. The CT oscillates in the $x-z$ plane. The origin is placed at the equilibrium position of CT (position of CT means the position of the center of the ferromagnetic particle).

Note that here we ignore the static displacement of the CT caused by the magnetic force of the spin. The magnetic moment of the spin, shown by the arrow in Fig. 1, points initially in the direction of the magnetic field B_0 , which corresponds to the equilibrium position of CT (see Eq. (4)). We assume now that the rf magnetic field $2B_1$ is linearly polarized in the plane which is perpendicular to B_0 (later we will discuss an arbitrary direction of polarization). The dipole magnetic field B_d is given by:

$$B_d = \frac{0}{4} \frac{3(m - n)n - m}{r_v^3}; \quad (1)$$

where m is the magnetic moment of the ferromagnetic particle pointing in the positive z -direction, r_v is the (variable) distance between the moving CT and the stationary spin, n is the unit vector pointing from the CT to the spin. We put:

$$r_v = \sqrt{(x - x_c)^2 + y^2 + z^2}; \quad (2)$$

$$n = \frac{x - x_c}{r_v}; \frac{y}{r_v}; \frac{z}{r_v}; \quad (3)$$

where x, y, z are the spin coordinates, and x_c is the CT-coordinate (i.e. the coordinate of the center of the ferromagnetic particle). In the state of equilibrium the net magnetic field on the spin is given by:

$$B_0 = B_{\text{ext}} + B_d^{(0)}; \quad (4)$$

$$B_d^{(0)} = \frac{3m_0}{4r^5} (zx, zy, z^2 - \frac{r^2}{3}); \quad (5)$$

$$B_{\text{ext}} = (0, 0, B_{\text{ext}}); \quad (6)$$

where $r = \sqrt{x^2 + y^2 + z^2}$. In the linear approximation on x_c the magnetic field B_d changes by the value of $B_d^{(1)}$:

$$B_d^{(1)} = (G_x, G_y, G_z) x_c; \quad (7)$$

$$(G_x, G_y, G_z) = \frac{3m_0}{4r^7} (z(r^2 - 5x^2), 5xyz, x(r^2 - 5z^2)); \quad (8)$$

where (G_x, G_y, G_z) describes the gradient of the magnetic field at the spin location at $x_c = 0$:

$$(G_x, G_y, G_z) = \left(\frac{\partial B_d}{\partial x}, \frac{\partial B_d}{\partial y}, \frac{\partial B_d}{\partial z} \right); \quad (9)$$

Note that the magnetic field and its gradient depend on the CT coordinate x_c . Next we consider the equation

of motion for the spin magnetic moment \sim in the system of coordinates rotating with the rf field of frequency ω about the magnetic field B_0 (the z axis of this new system points in the direction of B_0). We have:

$$\begin{aligned} \sim &= \sim B_{\text{eff}}; \\ B_{\text{eff}} &= (B_1, 0, B_0) (\omega =) \times_i G_i \cos_i; \\ \cos_i &= B_0^i = B_0; \end{aligned} \quad (10)$$

Here i , ($i = x, y, z$) are the angles between the direction of the magnetic field B_0 and the axes x, y, z of the laboratory system of coordinates, ω is the gyromagnetic ratio of the electron spin (ω is the absolute value of the gyromagnetic ratio). Note that we ignore the transversal components of the dipole field B_d as they represent the fast oscillating terms in the rotating system of coordinate. Also we consider only rotating component of the rf magnetic field.

The equations of motion for CT can be represented as follows:

$$x_c + !_c^2 x_c = F_x = m; \quad (11)$$

where $!_c$ and m are the frequency and the effective mass of the CT, F_x is the magnetic force acting on the ferromagnetic particle on CT. Note that we consider CT oscillations in the laboratory system of coordinates. Ignoring fast oscillating terms in the laboratory system, we obtain:

$$F_x = \frac{x}{z} G_i \cos_i; \quad (12)$$

Next, we will use the following units: for time $1 = !_c$, for magnetic moment B , for magnetic field $!_c =$, for length the characteristic distance L_0 between CT and the spin, for force $k_c L_0$, where $k_c = m !_c^2$ is the effective CT spring constant. Using these units, we derive the dimensionless equations of motion:

$$\begin{aligned} \sim &= \sim B_{\text{eff}}; \\ x_c + x_c &= F_x; \\ B_{\text{eff}} &= (B_1, 0, G x_c); \\ F_x &= G z; \\ &= B_0 \omega; \\ G &= \frac{1}{r^7} [z(r^2 - 5x^2) \cos x - 5xyz \cos y \\ &+ x(r^2 - 5z^2) \cos z]; \end{aligned} \quad (13)$$

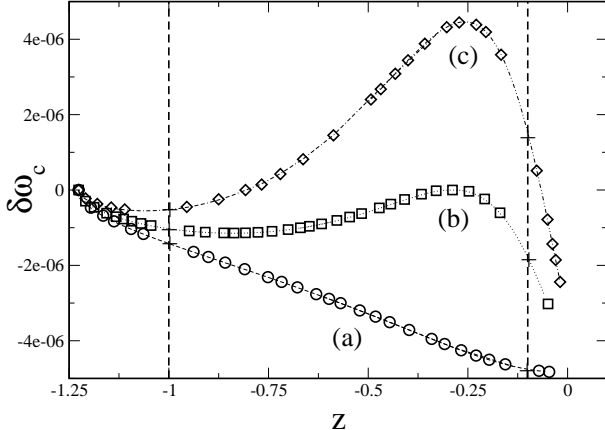


FIG. 2: The OSCAR M RFM frequency shift $\delta\omega_c(z)$ at the central resonant surface ($\gamma = 0$), for $x > 0$. Symbols show numerical data, lines correspond to estimate (17) for (a) $y = 0$ (circles), (b) $y = x = 2$ (squares) and (c) $y = x$ (diamond). Pluses indicate frequency shifts at the spin locations indicated in Fig. 3. In all figures the coordinates x, y and z are in units of L_0 and the frequencies are in units of ω_c .

Parameters and are given by:

$$= \frac{B_d \omega_c}{k_c L_0^2}; \quad = \frac{3}{4} \frac{\omega_m}{\omega_c L_0^3}; \quad (14)$$

Note that all quantities in Eq.(13) are dimensionless, i.e. x means $x = L_0$, m means $= B$, B_0 means $B_0 = \omega_c$ and so on. In terms of dimensional quantities the parameter equals the ratio of the dipole frequency $B_d^{(0)}$ to the CT frequency ω_c , and the product equals the ratio of the static CT displacement $F_x = k_c$ to the CT-spin distance L_0 . The derived equations are convenient for both numerical simulations and analytical estimations.

III. OSCAR M RFM FREQUENCY SHIFT

In this section we present the analytical estimate and the numerical simulations for the OSCAR M RFM frequency shift. When the CT oscillates, the resonant condition $\gamma = \mathcal{B}_{\text{ext}} + B_d j$ can be satisfied only if the spin is located inside the resonant slice which is defined by its boundaries:

$$\mathcal{B}_{\text{ext}} + B_d(x_c = A)j = \gamma = ; \quad (15)$$

where A is the amplitude of the CT vibrations. For an analytical estimate we assume that the spin is located at the central surface of the resonant slice. In this case in Eq.(13) $\gamma = 0$.

To obtain the analytical estimate for the OSCAR M RFM frequency shift we will assume an ideal adiabatic motion and put $\dot{\gamma} = 0$ in Eq.(13). Let the CT start its motion (at $t = 0$) from the right end position $x_c(0) = A$.

Then the initial direction (i.e. at $t = 0$) of the effective magnetic field \mathcal{B}_{eff} relative to the magnetic field $\mathcal{B}_{\text{ext}} + B_d j$ and of the magnetic moment \sim depends on the sign of G : \mathcal{B}_{eff} and \sim have the same direction for $G < 0$ and opposite direction for $G > 0$. Substituting the derived expression for $\gamma' = \mathcal{B}_{\text{eff}}^2 G = \mathcal{B}_{\text{eff}} j \mathcal{B}_{\text{ext}} j$ into F_x we obtain the following equation for x_c :

$$x_c + x_c \frac{1 + \frac{p}{1 + \frac{2Gj}{B_1^2 + (GA)^2}}}{1 + \frac{p}{2B_1^2 + (GA)^2}} = 0; \quad (16)$$

We solve this equation as in [3], using the perturbation theory of Bogoliubov and Mstropolsky [5], and we find the dimensionless frequency shift (see Appendix):

$$\omega_c' = \frac{2}{p} \frac{2Gj}{B_1^2 + (GA)^2} f(1 + \frac{1}{2} \frac{B_1^2}{2B_1^2 + (GA)^2} \ln \frac{p}{4} \frac{B_1^2 + (GA)^2}{B_1} + \frac{1}{2} i); \quad (17)$$

In typical experimental conditions we have

$$B_1 \ll GA;$$

and Eq.(17) transforms to a simple expression

$$\omega_c' = \frac{2}{A} \frac{G}{k_c}; \quad (18)$$

One can see that the frequency shift is determined by the ratio of the static CT displacement $F_x = k_c$ to the amplitude of the CT vibrations A . We will also present Eq.(17) in terms of dimensionless quantities:

$$\frac{\omega_c'}{\omega_c} = \frac{2}{A} \frac{G_0}{k_c}; \quad (19)$$

where

$$G_0 = \sum_i G_i \cos \phi_i; \quad (20)$$

Eqs.(17) and (19) represent an extension of the estimate derived in [3]. These equations are valid for any point on the central resonant surface and for any relation between \mathcal{B}_{ext} and $B_d j$. It follows from Eq.(17) that ω_c' is an even function of y and an odd function of x .

In our computer simulations we have used the parameters taken from experiments [2]:

$$\gamma = 2 = 5.5 \text{ kHz}; \quad k_c = 110 \text{ N/m}; \quad A = 16 \text{ nm};$$

$$\mathcal{B}_{\text{ext}} = 30 \text{ mT}; \quad \gamma = 2.96 \text{ GHz}; \quad \gamma = 106 \text{ mT};$$

$$\mathcal{B}_z j = 2 \times 10^5 \text{ T/m}; \quad B_1 = 300 \text{ T}; \quad L_0 = 350 \text{ nm};$$

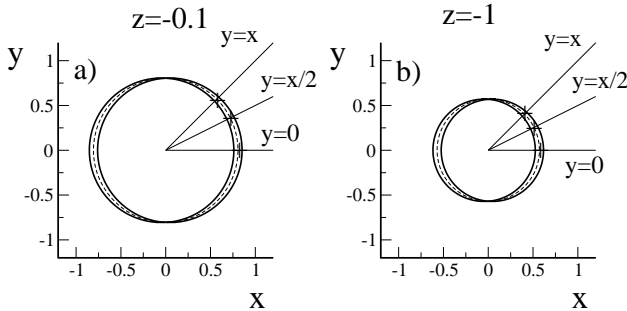


FIG . 3: a) and b) show s cross-sections of the resonant slice for $z = -0.1$ and $z = -1$. Dashed lines show the intersection between the cross section and the central resonant surface. Pluses indicate spin locations which correspond to the frequency shifts plot in Fig. 2.

The corresponding dimensionless parameters are the following:

$$= 1.35 \cdot 10^{13}; \quad = 1.07 \cdot 10^6; \quad A = 4.6 \cdot 10^2;$$

$$B_1 = 1.5 \cdot 10^3; \quad B_{\text{ext}} = 1.53 \cdot 10^5; \quad ! = 5.4 \cdot 10^5;$$

The initial conditions in our simulations are taking as

$$\sim(0) = (0; 0; 1);$$

$$x_c(0) = A; \quad x_c(0) = 0;$$

Below we describe the results of our computer simulations. Fig. 2 shows the frequency shift $!_c$ as a function of the spin z -coordinate at the central resonant surface ($= 0$). First, one can see an excellent agreement between the numerical data and the analytical estimate (17). Second, as it may be expected, the maximum magnitude of the frequency shift $j!_c j$ can be achieved when the spin is located in the plane of the CT vibrations $y = 0$. However, for $y = x$, it has almost the same magnitude $j!_c j$ (with the opposite sign of $!_c$). Moreover, for $y = x$ the dependence $!_c(z)$ has an extremum, which can be used for the measurement of the spin z -coordinate. If the distance between the CT and the surface of the sample can be controlled, then the "depth" of the spin location below the sample surface can be determined. (In all Figures, the coordinates x, y and z are given in units of L_0 , and the frequency shift is in units of $!_c$.)

Fig. 3 shows the cross-sections of the resonant slice for $z = -0.1$ and $z = -1$. The greater distance from the CT, the smaller the cross-sectional area. The asterisks in Fig. 3 show the spin locations, which correspond to the frequency shifts indicated by the asterisks in Fig. 2.

Fig. 4 demonstrates the "radial" dependence of the frequency shift $!_c(r_p)$, where $r_p = (x^2 + y^2)^{1/2}$. The value of r_p can be changed by the lateral displacement of the cantilever. As one may expect, the maximum value

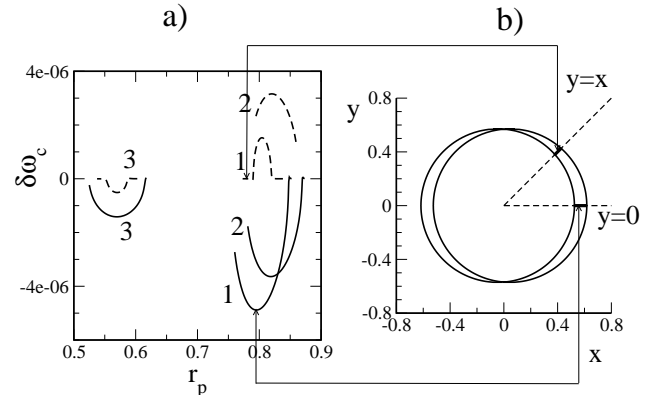


FIG . 4: (a) The OSCAR M R F M frequency shift $!_c(r_p)$ inside the cross-sectional area of the resonant slice for $x > 0$. Solid lines correspond to $y = 0$, dashed lines correspond to $y = x$. Lines are (1), $z = -0.1$, (2), $z = -0.43$, and (3), $z = -1$. $\xi = (x^2 + y^2)^{1/2}$. (b) Cross-section of the resonant slice $z = -0.1$. Bold segments show the spin locations which correspond to the lines (1) on (a).

of $j!_c j$ corresponds to the central resonant surface. The maximum becomes sharper as z decreases. Thus, the small distance between the CT and the sample surface is preferable for the measurement of the radial position of the spin.

Fig. 5 shows the "azimuthal dependence" of the frequency shift $!_c()$, where $= \tan^{-1}(y/x)$ and the spin is located on the central resonant surface. Note that for the given values of z and $$, the coordinates x and y of the spin are fixed, if the spin is located on the central resonant surface. The value of $$ can be changed by rotating the cantilever about its axis. One can see the sharp extremum of the function $!_c()$. Again, the small distance between the CT and the sample is preferable for the measurement of the "azimuthal position" of the spin.

Finally, we consider the realistic case when the direction of polarization of the rf field $2B_1$ is fixed in the laboratory system of coordinate. Now the angle between the direction of polarization of $2B_1$ and the field B_0 depends on the spin coordinate as the magnitude and the direction of the dipole field $B_d^{(0)}$ depend on the spin location. To describe this case we ignore the component of $2B_1$, which is parallel to B_0 , and change B_1 to $B_1 \sin \theta$ in all our formulas. As an example, Fig. 6 demonstrates the dependence $!_c(z)$ for the case when the rf field is polarized along the x -axis. One can see that in a narrow region of z the magnitude of the frequency shift sharply drops. It happens because in this region the magnetic field B_0 is almost parallel to the x -axis. Thus, the effective field $B_1 \sin \theta$ is small, the condition of the adiabatic motion $|B_1 \sin \theta| \gg \mu B_{\text{eff}} = dt/dz$ is not satisfied, and the spin does not follow the effective magnetic field. Dashed lines in Fig. 6 correspond to the analytical estimate (17) with the substitution $B_1 = B_1 \sin \theta$: the analytical estimate assumes adiabatic conditions, which are violated

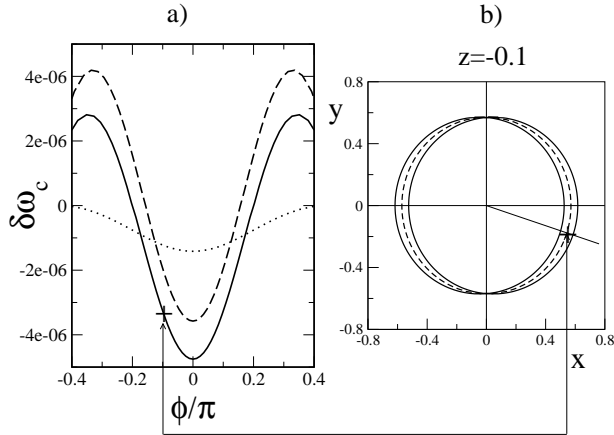


FIG. 5: a) Dependence $\delta\omega_c(\phi)$, with $\phi = \tan^{-1}(y/x)$ for the central resonant surface and $z = 0.1$ (full line); $z = 0.4$ (dashed line), $z = 1$ (dotted line). b) solid line shows the cross-section of the resonant slice for $z = 0.1$. Dashed line shows the intersection between the plane $z = 0.1$ and the central resonant surface. The plus in (b) shows the spin location $z = 0.1$. The corresponding frequency shift is marked by a plus on (a).

for small θ .

The sharp drop of $j\delta\omega_c$ could be observed either by the change of the distance between the CT and the sample surface or by the change of the direction of polarization of the rf field.

In any case this effect could be used for independent measurement of the spin "depth" below the sample surface.

IV. CONCLUSION

We have derived the quasiclassical equations of motion describing the OSCAR technique in MRFM for arbitrary relation between the external and dipole magnetic fields and arbitrary location of a single spin. We have obtained the analytical estimate for the OSCAR MRFM frequency shift $\delta\omega_c$, which is in excellent agreement with numerical simulations. We have shown that the dependence $\delta\omega_c$ on the position of spin relative to the cantilever contains characteristic maxima and minima which can be used in order to determine the position of the spin. We believe that moving cantilever in three dimensions, rotating it about its axis and changing the direction of the polarization of the rf magnetic field, experimentalist eventually will be able to determine the position of a single spin. We hope that our work will help to achieve this goal.

Acknowledgments

This work was supported by the Department of Energy (DOE) under Contract No. W-7405-ENG-36, by the De-

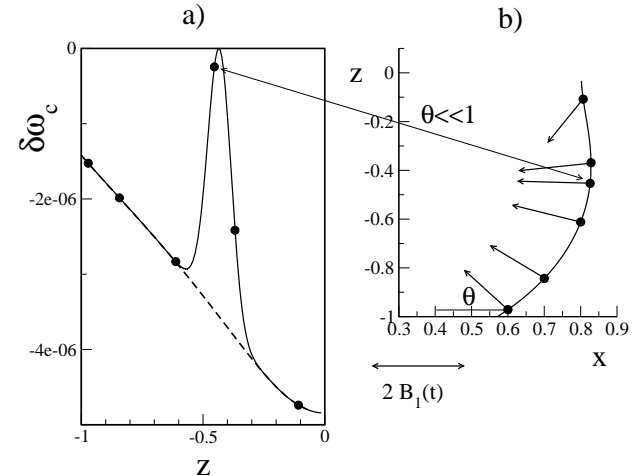


FIG. 6: (a) dependence $\delta\omega_c(z)$ when the rf field B_1 is parallel to the x-axis. The spin is located at the central resonant surface $y = 0$, $x > 0$. Solid line are numerical data, dashed line is the analytical estimate (17), which assumes adiabatic motion of the spin magnetic moment \sim parallel to B_{eff} . For a few numerical points indicated as closed circles in (a) the corresponding B_0 field is shown in (b). (b) solid line: intersection between the central resonant surface and the x - z plane. Arrows show the magnetic field B_0 on this intersection at the points indicated as closed circles in (a). The absolute value of the frequency shift $j\delta\omega_c$ drops at the spin locations where B_0 is approximately parallel to B_1 ($\theta \approx 1$).

Defense Advanced Research Projects Agency (DARPA), by the National Security Agency (NSA), and by the Advanced Research and Development Activity (ARDA).

V. APPENDIX

Eq. (16) can be written in the following form:

$$\frac{d^2 x_c}{dt^2} + x_c = f(x_c); \quad (21)$$

where $t = \delta\omega_c t$ is the dimensionless time,

$$f(x_c) = P \frac{Gx_c}{B_1^2 + (G)^2 x_c^2}; \quad (22)$$

and $P = Gj$.

The approximate solution of (21), can be written as [5]:

$$x_c(t) = a(t) \cos(\omega t) + O(t); \quad (23)$$

where in the first order in t , $a(t)$ and $\omega(t)$ satisfy the equations:

$$\begin{aligned} \frac{da}{dt} &= P_1(a) + O(t); \\ \frac{d\omega}{dt} &= 1 + Q_1(a) + O(t); \end{aligned} \quad (24)$$

and the functions $P_1(a)$ and $Q_1(a)$ are given by:

$$P_1(a) = \frac{1}{2} \int_0^{Z_2} f(a \cos \phi) \sin \phi d\phi; \quad (25)$$

$$Q_1(a) = \frac{1}{2a} \int_0^{Z_2} f(a \cos \phi) \cos \phi d\phi; \quad (26)$$

On inserting the explicit expression (22) for $f(a \cos \phi)$ one gets:

$$P_1(a) = 0; \quad (27)$$

$$Q_1(a) = -\frac{2G}{p} \int_0^{Z_2} \frac{(1 - \sin^2 \phi)}{1 - k^2 \sin^2 \phi} d\phi; \quad (28)$$

where

$$k^2 = \frac{(Ga)^2}{B_1^2 + (Ga)^2}; \quad (29)$$

Eq.(28) can be written as:

$$Q_1(a) = -\frac{2G}{k^2} \int_0^{Z_2} \frac{1}{B_1^2 + (Ga)^2} [(k^2 - 1)K(k) + E(k)]; \quad (30)$$

where $K(k)$ and $E(k)$ are the complete elliptic integrals of the first and second kind. When $k^2 \ll 1$ elliptic integrals can be approximated by:

$$K(k) \approx \ln p \frac{4}{1 - k^2} + \frac{1}{4} \ln p \frac{4}{1 - k^2} - \frac{1}{2} (1 - k^2); \quad (31)$$

$$E(k) \approx 1 + \frac{1}{2} \ln p \frac{4}{1 - k^2} - \frac{1}{2} (1 - k^2); \quad (32)$$

In the first order approximation the frequency shift is:

$$!_c \approx Q_1(a) = -\frac{2}{p} \frac{2G \mathfrak{G} j}{B_1^2 + (Ga)^2} f_1 + \frac{1}{2} \frac{B_1^2}{B_1^2 + (Ga)^2} \ln \frac{4}{B_1^2 + (Ga)^2} + \frac{1}{2} i; \quad (33)$$

In our approximation $a = A$ that gives Eq. (17).

[1] B.C. Stipe, H.J. Mamin, C.S. Yannoni, T.D. Stowe, T.W. Kenny and D. Rugar, Phys. Rev. Lett. 87, 277602 (2001).

[2] D. Rugar, R. Budakian, H.J. Mamin and B.W. Chui, Nature 430, 329 (2004).

[3] G.P. Berman, D.I. Kamenev and V.I. Tsifrinovich, Phys. Rev. A 66, 023405 (2002).

[4] G.P. Berman, F. Boronov and V.I. Tsifrinovich, Quantum Information and Computation, 4, 102 (2004).

[5] N.N. Bogolubov and Y.A. Mitropolsky, Asymptotic methods in the theory of non-linear oscillations, (translated from Russian), Delhi, Hindustan Pub. Corp. (1961).